HHS Public Access

Author manuscript

Neuron. Author manuscript; available in PMC 2017 December 07.

Published in final edited form as:

Neuron. 2016 December 07; 92(5): 1020–1035. doi:10.1016/j.neuron.2016.10.014.

Actin is crucial for all kinetically distinguishable forms of endocytosis at synapses

Xin-Sheng Wu[1,*], **Sunghoon Lee**[1,*], **Jiansong Sheng**[1,◆], **Zhen Zhang**[1,2,◆], **Weidong Zhao**[1], **Dongsheng Wang**[1], **Yinghui Jin**[1], **Patrick Charnay**[3], **James M. Ervasti**[4], and **Ling-Gang Wu**[1,◆,5]

[1]National Institute of Neurological Disorders and Stroke, 35 Convent Dr., Bethesda, MD 20892

[3]Ecole normale supérieure, PSL Research University, CNRS, Inserm, Institut de Biologie de l'Ecole normale supérieure, F-75005 Paris, France

[4]Department of Biochemistry, Molecular Biology and Biophysics, University of Minnesota, Minneapolis, MN 55455

Summary

Mechanical force is needed to mediate endocytosis. Whether actin, the most abundant force-generating molecule, is essential for endocytosis is highly controversial in mammalian cells, particularly synapses, likely due to the use of actin blockers, the efficiency and specificity of which are often unclear in the studied cell. Here we addressed this issue using knockout approach combined with measurements of membrane capacitance and fission pore conductance, imaging of vesicular protein endocytosis, and electron microscopy. We found that two actin isoforms, β- and γ-actin, are crucial for slow, rapid, bulk, and overshoot endocytosis at large calyx-type synapses, and for slow endocytosis and bulk endocytosis at small hippocampal synapses. Polymerized actin provides mechanical force to form endocytic pits. Actin also facilitates replenishment of the readily releasable vesicle pool, likely via endocytic clearance of active zones. We conclude that polymerized actin provides mechanical force essential for all kinetically distinguishable forms of endocytosis at synapses.

◆Correspondence: shengjs@gmail.com (J.S.), zhen0806@gmail.com (Z.Z.), wul@ninds.nih.gov (L.G.W).

[2]Current address: Office of Genetic Drugs, Center for Drug Evaluation and Research, Food and Drug Administration, 10903 New Hampshire Ave., Silver spring, MD 20993

[5]**Lead contact:** Ling-Gang Wu

[*]Co-first author

Author contributions

X.S.W., S.L., J.S. and Z.Z. performed and analyzed experiments. W.Z., D.W and Y.J. assisted some experiments. P.C. provided Krox20^{Cre} mice. J.M.E. provided Actb$^{LoxP/LoxP}$ and Actg1$^{LoxP/LoxP}$ mice. J.S., Z.Z. and L.G.W. designed experiments, supervised the project and wrote the paper with helps from other authors.

Introduction

Endocytosis, a fundamental biological process, relies on mechanical force to mediate membrane invagination, formation of the Ω-shaped membrane profile, and Ω-profile fission (Saheki and De Camilli, 2012). What molecule provides force for these steps is poorly understood. Actin, a force-generating molecule (Blanchoin et al., 2014), provides forces for endocytosis in yeast (Engqvist-Goldstein and Drubin, 2003). However, its role in mammalian cells has been highly controversial (Saheki and De Camilli, 2012). To our knowledge, all studies in mammalian cells rely on pharmacological blockers. In non-neuronal mammalian cells, studies reached different conclusions as to whether and which step actin is involved in endocytosis (Boulant et al., 2011; Ferguson et al., 2009; Merrifield et al., 2005; Saffarian et al., 2009; Yao et al., 2013; Yarar et al., 2005). A recent study proposes that actin dynamics is only needed on surfaces under tension, which offers an explanation for the conflicting results (Boulant et al., 2011). However, this explanation is difficult to account for the large scale of conflicts at synapses, as discussed below.

Latrunculin B, phalloidin, and swinholide A, which disrupt filamentous actin (F-actin) assemble/disassembly dynamics, cause accumulation of clathrin-coated pits and vesicles at lamprey giant synapses, suggesting a role of actin in endocytosis (Bourne et al., 2006; Shupliakov et al., 2002). However, at the same lamprey synapse, latrunculin A, which disrupts actin polymerization, does not affect endocytosis detected with FM1-43 uptake (Bleckert et al., 2012). Phalloidin, which stabilizes F-actin, reduces FM1-43 uptake and exocytosis to a similar extent, suggesting that phalloidin inhibits exo-, but not endocytosis (Bleckert et al., 2012). At frog neuromuscular junctions, latrunculin A reduces FM1-43 uptake into nerve terminals (Richards et al., 2004). While this observation could be interpreted as inhibition of endocytosis, it may reflect inhibition of exocytosis, because latrunculin A reduces both exocytosis and FM1-43 uptake to a similar extent (Richards et al., 2004). Furthermore, cytochalasin D, which inhibits actin polymerization, does not affect FM1-43 uptake or release, questioning a role of actin in endocytosis at frog neuromuscular junctions (Betz and Henkel, 1994). At hippocampal synapses, latrunculin A slows down spontaneous vesicle endocytosis (Hua et al., 2011a) and ultrafast endocytosis after single action potentials (Watanabe et al., 2014), but does not affect endocytosis or the recycling pool after action potential trains (Hua et al., 2011b; Li and Murthy, 2001; Sankaranarayanan et al., 2003), raising the possibility that actin's role is limited to minimal stimulation. At goldfish retinal bipolar synapses, cytochalasin D does not affect vesicle recycling as detected with FM1-43 uptake and release (Job and Lagnado, 1998); latrunculin B and cytochalasin D do not affect endocytosis with a time course < ~20 s, but slow down bulk endocytosis (Holt et al., 2003), questioning a general role of actin in all forms of endocytosis. A recent study showed that latrunculin A inhibits fast endocytosis at mossy fiber boutons (Delvendahl et al., 2016), consistent with inhibition of ultrafast endocytosis at hippocampal synapses (Watanabe et al., 2014). In summary, the effects of actin blockers obtained at the same synapse, at different synapses, and for different forms of endocytosis are controversial.

The present work aimed at determining whether actin is essential for various forms of endocytosis across different synapses and how actin acts on endocytosis. Since all previous studies rely on actin blockers, and some use only one blocker at one concentration, false–

positive or –negative results due to off-target effects or difficulty of drug access to actin in the *in vivo* condition (Bleckert et al., 2012) might contribute to the controversy. In the present work, we used the conditional actin gene knockout approach to study actin's endocytic role in mammalian cells for the first time. Among six actin isoforms in mammalian cells, β-cytoplasmic actin (β-actin) encoded by *Actb* and γ-cytoplasmic actin (γ-actin) encoded by *Actg1* are ubiquitously expressed (Herman, 1993), and are the predominant isoforms in the brain (Cheever and Ervasti, 2013). Since global knockout of β-actin is lethal (Shawlot et al., 1998; Shmerling et al., 2005), we generated mice with β-actin or γ-actin knockout specifically at calyx of Held and hippocampal synapses. We chose calyces, because four kinetically different forms of endocytosis, including slow clathrin-dependent endocytosis (tens of seconds), rapid, presumably clathrin-independent endocytosis (a few seconds), bulk endocytosis (retrieving vesicles larger than regular vesicles), and endocytosis overshoot (retrieving more vesicles than exocytosed), can be recorded with capacitance measurements (Wu et al., 2014a). We chose hippocampal synapses, because we can determine whether results obtained at large calyces apply to small conventional synapses, and electron microscopy can be used to determine the ultrastructural changes. Our results suggest that actin is essential in mediating all kinetically different forms of endocytosis by providing mechanical force to generate endocytic pits.

Results

β- and γ-actin knockout at calyces

We knocked out β-actin or γ-actin tissue-specifically using krox20^{Cre} mice, where krox20-driven Cre activity is limited to the lower auditory system, including calyces and postsynaptic neurons in the medial nucleus of the trapezoid body (MNTB) (Han et al., 2011). Breeding Krox20^{Cre} mice with zsGreen reporter mice (Jacskon lab) (Madisen et al., 2010) yielded Krox20$^{Cre/+}$; zsGreen$^{+/-}$ mice, in which zsGreen fluorescence overlapped with all 136 calyces (2 mice) labelled with vesicular glutamate transporter 1 (vGluT$_1$, Fig. S1A–B). This result further supports the finding that Cre is present in calyx-containing neurons in krox20^{Cre} mice (Han et al., 2011). Breeding Krox20$^{Cre/+}$ mice with Actb$^{LoxP/LoxP}$ mice, and subsequent breeding of Krox20$^{Cre/+}$; Actb$^{LoxP/+}$ mice with Actb$^{LoxP/LoxP}$ mice yielded Krox20$^{Cre/+}$; Actb$^{LoxP/LoxP}$ mice (Actb$^{-/-}$), in which β-actin was deleted in calyces. Similarly, we generated Krox20$^{Cre/+}$; Actg1$^{LoxP/LoxP}$ mice (Actg1$^{-/-}$) to delete γ-actin. Since calyces from Actb$^{LoxP/LoxP}$ mice, Actg1$^{LoxP/LoxP}$ mice, and wild-type mice exhibit similar properties (not shown), we group these mice together as control mice.

In control mice, immunostaining showed that β- and γ-actin were co-localized with vGluT$_1$ that labeled vesicles in P7-10 calyces (Fig. 1A–B). Similar labeling was observed at more mature P13-14 calyces (Fig. S1C–F), indicating the presence of β- and γ-actin throughout P7-14. In Actb$^{-/-}$ or Actg1$^{-/-}$ mice, β- or γ-actin was nearly absent at P7-10 calyces, respectively (Fig. 1A–B). The remaining immunostaining was close to background staining (Fig. 1A–B). These results suggest that krox20^{Cre} successfully deleted β- or γ-actin in Actb$^{-/-}$ or Actg1$^{-/-}$ calyces, respectively. Deletion of β-actin in Actb$^{-/-}$ mice did not significantly affect expression of γ-actin (Fig. 1A–B), or dynamin and syndapin that may

interact with actin, in calyces (Fig. S2). Similarly, β-actin expression did not change significantly in Actg1$^{-/-}$ calyces (Fig. 1A–B).

We also bred Actb$^{-/-}$ and Actg1$^{-/-}$ mice to generate β- and γ-actin double knockout mice (Krox20$^{Cre/+}$; Actb$^{LoxP/LoxP}$; Actg1$^{LoxP/LoxP}$ mice, or DKO mice). DKO mice were smaller than controls, but survived beyond P7-10. However, no calyces can be identified, suggesting that actin is required for calyx development.

Actin is involved in slow endocytosis

We induced slow endocytosis (τ > ~10 s) by applying a 20 ms depolarization from −80 mV to +10 mV (depol$_{20ms}$) to calyces at the whole-cell voltage-clamp configuration (Wu et al., 2009). If not mentioned, recordings were made in P7-10 calyces at 22–24°C. Depol$_{20ms}$ induced a calcium current (ICa) of 1.6 ± 0.1 nA and a capacitance (Cm) jump (ΔCm) of 362 ± 23 fF in control mice (n = 13 calyces, 13 mice, Fig. 2A–C). ΔCm was followed by a mono-exponential decay with a τ of 15.9 ± 1.9 s and an initial decay rate (Rate$_{decay}$) of 28 ± 4 fF/s (n = 13, Fig. 2A–C). Although both τ and Rate$_{decay}$ reflected endocytosis rate, we used Rate$_{decay}$ for statistics (Sun et al., 2010; Wu et al., 2009), because the decay τ was often too slow to estimate in knockout mice.

The Rate$_{decay}$ in Actb$^{-/-}$ (12 calyces, 8 mice) or Actg1$^{-/-}$ calyces (12 calyces, 9 mice) was reduced to ~17–24% of control ($p < 0.01$), whereas ICa charge (QICa) and ΔCm were not different (Fig. 2A–C, $p > 0.1$). Similar reduction was observed when 1) depol$_{20ms}$ was replaced with 20 action potential-equivalent stimuli (APe, 1 ms from −80 to +7 mV) (Wu et al., 2009) at 100 Hz, which also induced slow endocytosis in control mice (Fig. 2D–F), 2) the temperature was increased to 34–37°C for 15–20 min (Fig. 2G), or 3) P7-10 was changed to P13-14 (Fig. 2H), at which calyces are more matured (Borst and Soria van Hoeve, 2012). Thus, inhibition of slow endocytosis by β- or γ-actin knockout is independent of the stimulation protocol, temperature, or developmental stage, suggesting involvement of actin in slow endocytosis.

We noticed that endocytosis was not fully blocked by β-actin knockout (Fig. 2G–H). This could be due to the presence of other actin isoforms like γ-actin. In control calyces, Rate$_{decay}$ after depol$_{20ms}$ at 34–37°C for 15–20 min (67 ± 13 fF/s, n = 8, Fig. 2G) was significantly higher than that (28 ± 4 fF/s, n = 13, Fig. 2A–C) observed at 22–24°C ($p < 0.01$, t test), consistent with the temperature-dependent acceleration of endocytosis observed at calyces and mossy fiber boutons (Delvendahl et al., 2016; Renden and von Gersdorff, 2007). In addition, ICa at 34–37°C was faster in kinetics and larger in amplitude (Fig. S3), consistent with previous observations (Renden and von Gersdorff, 2007).

Actin is involved in rapid endocytosis

We applied 10 depol$_{20ms}$ at 10 Hz (depol$_{20msX10}$) to induce rapid endocytosis (Wu et al., 2009). In control calyces (P7-10, 22–24°C), depol$_{20msX10}$ induced a ΔCm of 1045 ± 53 fF, followed by a bi-exponential decay with τ of 1.7 ± 0.2 s (21 ± 2%) and 21.6 ± 1.4 s (n = 13, Fig. 3A–B), respectively. The Rate$_{decay}$ was 180 ± 26 fF/s (n = 13, Fig. 3C), which reflected mostly (~80%) the rapid component of endocytosis (Sun et al., 2010; Wu et al., 2009). The Rate$_{decay}$ in Actb$^{-/-}$ (n = 12 calyces, 8 mice) and Actg1$^{-/-}$ calyces (n = 12 calyces, 9 mice)

decreased to ~20–22% of that in control ($p < 0.01$), whereas QICa did not change significantly (Fig. 3A–C). ΔCm induced by $depol_{20msX10}$ was 890 ± 95 fF (n = 12) and 795 ± 80 fF (n = 12) in $Actb^{-/-}$ and $Actg1^{-/-}$ calyces, respectively, which was ~75–84% of control (Fig. 3A–C, $p < 0.05$). Such a small ΔCm reduction is insufficient to account for the large $Rate_{decay}$ decrease, because theoretically the initial Cm decay rate is equal to ΔCm divided by the τ of the mono-exponential Cm decay. If τ does not change, a decrease of ΔCm to 77–84% of control should linearly decrease the $Rate_{decay}$ to ~77–84% of control, but not the observed 20–22% of control. Thus, reduction of $Rate_{decay}$ is largely not caused by ΔCm decrease, consistent with studies showing that block of endocytosis is not due to exocytosis decrease (reviewed in Wu et al., 2014a).

Similar reduction of $Rate_{decay}$ in $Actb^{-/-}$ or $Actg1^{-/-}$ calyces was observed when 1) $depol_{20msX10}$ was replaced with 200 APe at 100 Hz, which also induced rapid endocytosis in control (Sun et al., 2010; Wu et al., 2009) (Fig. 3D–F), 2) the temperature was increased to 34–37°C (Fig. 3G), or 3) P7-10 was changed to P13-14 (Fig. 3H). These results suggest the involvement of actin in rapid endocytosis.

Reduction of $Rate_{decay}$ is not due to asynchronous release that counteracts endocytosis for two reasons. First, with 1 mM EGTA in the pipette to block calcium-dependent asynchronous release, $Rate_{decay}$ after $depol_{20ms}$ or $depol_{20msX10}$ in $Actb^{-/-}$ calyces (n = 8) was still much slower than control (n = 7, Fig. S4). Second, the EPSC after 20 AP at 100 Hz decayed back to baseline within 1.5 s in both $Actb^{-/-}$ (n = 4) and control (n = 4) neurons (Fig. S5), whereas the Cm decay did not return to baseline in 40 s after 20 APe at 100 Hz in $Actb^{-/-}$ calyces (Fig. 2D). The prolonged Cm decay is thus not due to asynchronous release.

Actin is involved in bulk endocytosis

Bulk endocytosis is detected as a brief downward Cm shift (DCS) of ~20–500 fF at the whole-cell configuration (Wu and Wu, 2007), but can be down to 500 aF at the cell-attached configuration (He et al., 2009). We induced DCSs with 10 pulses of 50 ms depolarization from −80 to +10 mV at 10 Hz ($depol_{50msX10}$) with 5.5 mM Ca^{2+} in the bath at the whole-cell configuration (Wu et al., 2009). In control calyces, the DCS frequency measured every 20 s was 0.0044 ± 0.0028 Hz at rest, but increased to 0.0246 ± 0.0050 Hz (n = 24 calyces, 18 mice) within 20 s after $depol_{50msX10}$ ($p < 0.01$), and returned to baseline in the next 20 s (Fig. 4A–B), consistent with previous reports (Wu and Wu, 2007; Wu et al., 2009). The DCS frequency within 20 s after $depol_{50msX10}$ was only ~25% of control in $Actb^{-/-}$ mice (n = 29 calyces, $p < 0.01$), and ~19% in $Actg1^{-/-}$ mice (n = 18 calyces, $p < 0.01$) (Fig. 4A–B). The DCS size did not change significantly (not shown). Thus, bulk endocytosis is inhibited in $Actb^{-/-}$ and $Actg1^{-/-}$ mice.

During DCSs, the fission pore conductance (G_p) changes can be measured (Fig. 4C), allowing us to dissect endocytosis into two steps, the formation of an Ω-profile with a fission pore, and fission pore closure (Wu and Wu, 2007). G_p at the DCS onset that reflects initial fission pore size, and the rate of G_p change during DCS that reflects fission pore closure rate, were similar in control, $Actb^{-/-}$ and $Actg1^{-/-}$ calyces (Fig. 4C–D), suggesting that actin knockout may inhibit formation of the Ω-profile.

Actin is involved in endocytosis overshoot

Endocytosis overshoot (Renden and von Gersdorff, 2007) can be reliably induced by $depol_{50msX10}$ with 5.5 mM Ca^{2+} in the bath (Xue et al., 2012). $Depol_{50msX10}$ induced an endocytosis overshoot of 620 ± 132 fF (n = 24 calyces) in control mice (e.g., Fig. 4A; averaged in Fig. 5A, left), but did not induce overshoot in $Actb^{-/-}$ (29 calyces, e.g., Fig. 4C; averaged in Fig. 5A, middle) or $Actg1^{-/-}$ mice (18 calyces, e.g., Fig. 4E; averaged in Fig. 5A, right). These results (summarized in Fig. 5B) suggest that β- and γ-actin are required for endocytosis overshoot. In addition, $Rate_{decay}$ after $depol_{50msX10}$ in $Actb^{-/-}$ and $Actg1^{-/-}$ mice was reduced substantially (Fig. 5C), similar to that observed after $depol_{20msX10}$ (Fig. 3).

Actin facilitates the RRP replenishment

In $Actb^{-/-}$ and $Actg1^{-/-}$ calyces, ΔCm was reduced after $depol_{20msX10}$ or 200 APe at 100 Hz (Fig. 3), but not after $depol_{20ms}$ or 20 APe at 100 Hz (Fig. 2). Since $depol_{20ms}$ or 20 APe at 100 Hz depleted the readily releasable vesicle pool (RRP) (Sun and Wu, 2001), the RRP must be repeatedly depleted and refilled during $depol_{20msX10}$ or 200 APe at 100 Hz (Wu et al., 2009). ΔCm reduction after $depol_{20msX10}$ or 200 APe at 100 Hz may thus reflect slower RRP replenishment. Consistently, the accumulated ΔCm from the 2^{nd} to the 10^{th} $depol_{20ms}$ during $depol_{20msX10}$ in $Actb^{-/-}$ and $Actg1^{-/-}$ calyces was significantly smaller than control (Fig. 5D–E). When a pair of $depol_{20ms}$ was applied at various intervals, the ratio between the 2^{nd} and the 1^{st} ΔCm recovered more slowly in $Actb^{-/-}$ calyces than in control (Fig. 5F–G), suggesting that actin knockout inhibits RRP replenishment. In other words, actin facilitates RRP replenishment, consistent with a report that actin blockers inhibit RRP replenishment (Sakaba and Neher, 2003).

Inhibition of endocytosis by the block of dynamin, calmodulin, calcium influx, and SNARE proteins slows down RRP replenishment, suggesting that endocytosis may facilitate RRP replenishment by clearance of the active zone perturbed by exocytosis (Neher, 2010; Wu et al., 2014a). Actin may facilitate RRP replenishment via facilitation of active zone clearance.

Actin is involved in slow endocytosis at hippocampal synapses

We expressed Cre with three methods to delete actin gene in hippocampal synapses. First, we cultured hippocampal synapses from $Actb^{LoxP/LoxP}$ or $Actg1^{LoxP/LoxP}$ mice. Infection of hippocampal cultures with lentivirus containing a Cre enzyme for ≥ 7 days led to deletion of β- or γ-actin, respectively, as shown in western blot (Fig. 6A–B). Deletion of β- or γ-actin did not affect expression of major endocytic proteins, including clathrin heavy chain, dynamin, and adaptor protein 2 (AP2) (e.g., Fig. 6A–B, n = 3 experiments), suggesting that the effects of β- or γ-actin knockout are not due to reduction of these proteins.

Second, we generated $Cre\text{-}ER^{TM}$;$Actb^{LoxP/LoxP}$ mice by crossing *CAGGCre-EM*^{TM} mice, which contain tamoxifen-inducible cre-mediated recombination system in diverse tissues (Hayashi and McMahon, 2002), with $Actb^{LoxP/LoxP}$ mice. Hippocampal cultures from $Cre\text{-}ER^{TM}$;$Actb^{LoxP/LoxP}$ mice were treated with 4-OH-tamoxifen (TM, 1 μM). 2 and 4 days later, β-actin was reduced to 55 ± 5% and 13 ± 7% of control (0 day after TM application, Fig. 6C, n = 4 western blots), respectively, whereas γ-actin expression (103 ± 3% and 101

± 3%, n = 4) did not change significantly (Fig. 6C, $p > 0.3$). We did not generate Cre-ER^{TM};Actg1$^{LoxP/LoxP}$ mice, because either β- or γ-actin knockout produced similar effects (Figs. 2–5).

Third, for measuring endocytosis, we transfected the cultured Actb$^{LoxP/LoxP}$ or Actg1$^{LoxP/LoxP}$ neurons with SypH (synaptophysin tagged with the pH-sensitive pHluorin2X) (Zhu et al., 2009) either alone as control or with a plasmid containing Cre-mCherry for ≥ 7 days to generate Actb$^{-/-}$ or Actg1$^{-/-}$ boutons, respectively (mChery for recognition, Fig. 6D). Measurements were made at 22–24°C, if not mentioned otherwise. In control (SypH transfection alone, Fig. 6E), a 10 s train of stimulus (1 ms/20 mA) at 20 Hz ($Train_{10s}$), which induced an action potential train (Sankaranarayanan and Ryan, 2000; Sun et al., 2010), induced a SypH fluorescence (F_{SypH}) increase (ΔF) of 72 ± 7% of the baseline intensity (Fig. 6E, n = 8 experiments). ΔF was followed by a mono-exponential decay reflecting endocytosis with a τ of 23.4 ± 2.0 s and a $Rate_{decay}$ of 2.1 ± 0.1%/s (Fig. 6E–G, n = 8). A 2 s stimulation train ($Train_{2s}$) induced a ΔF of 28.0 ± 3.2%, followed by a decay with a τ of 13.9 ± 0.9 s and a $Rate_{decay}$ of 1.7 ± 0.3%/s (n = 5, Fig. 6E–G).

In Actb$^{-/-}$ neurons showing mCherry and SypH fluorescence (Fig. 6D), $Train_{10s}$ induced a ΔF of 22.5 ± 4.5%, followed by a decay with a $Rate_{decay}$ of 0.3 ± 0.1%/s (Fig. 6E–G, n = 11), which was only ~14% of that induced by $Train_{10s}$ in control or ~18% of that by $Train_{2s}$ in control (Fig. 6E–G, $p < 0.01$). Similarly, in Actg1$^{-/-}$ boutons showing mCherry and SypH fluorescence, $Train_{10s}$ induced a ΔF of 34.1 ± 10.8%, followed by a decay with a $Rate_{decay}$ of 0.8 ± 0.2%/s (Fig. 6E–G, n = 10), which was ~38–47% of that induced by $Train_{10s}$ or $Train_{2s}$ in control (Fig. 6E–G, $p < 0.01$). F_{SypH} decay, when normalized to the peak ΔF, was much slower in Actb$^{-/-}$ or Actg1$^{-/-}$ boutons than control (Fig. 6F).

Is the slower F_{SypH} decay due to slower re-acidification or endocytosis? In Actb$^{-/-}$ boutons, MES solution with a pH of 5.5 applied before $Train_{10s}$ quenched F_{SypH} to the background level and decreased F_{SypH} by ΔS (Fig. 6H), which reflected the pre-existing SypH molecules at the plasma membrane. Washing out MES solution led to recovery of F_{SypH} to baseline (Fig. 6H). We then applied $Train_{10s}$ and applied MES solution at 10 s after $Train_{10s}$, at which F_{SypH} was near the peak level. F_{SypH} was quenched to a level similar to that in MES solution before $Train_{10s}$ (lower dotted line, Fig. 6H), but much lower than that predicted if F_{SypH} decay is due to re-acidification (upper dotted line, Fig. 6H, n = 6). Quenched F_{SypH} recovered above baseline after MES washout, confirming the prolonged presence of SypH at the plasma membrane (Fig. 6H). Thus, slower F_{SypH} decay in Actb$^{-/-}$ boutons primarily reflected slower endocytosis.

In control boutons at 34–37°C, $Rate_{decay}$ after $Train_{10s}$ (5.0 ± 1.6%/s, n = 4, Fig. 6I) was significantly higher than that at 22–24°C (2.1 ± 0.1%/s, n = 8, Fig. 6E, G; $p < 0.01$, t test), consistent with the temperature-dependent increase of endocytosis observed rat hippocampal synapses (Micheva and Smith, 2005). Compared to control at 34–37°C, F_{SypH} decay and $Rate_{decay}$ after $Train_{10s}$ in Actb$^{-/-}$ boutons were much slower (Fig. 6I, n = 5), suggesting that actin knockout inhibits endocytosis at both 22–24°C and 34–37°C.

ΔF (normalized to baseline F_{SypH}) induced by $Train_{10s}$ in $Actb^{-/-}$ or $Actg1^{-/-}$ boutons was smaller than control (Fig. 6E, G), suggesting a reduction of exocytosis, because baseline F_{SypH} did not change in $Actb^{-/-}$ (Fig. S6A) or $Actg1^{-/-}$ (not shown) boutons. Furthermore, when we normalized ΔF to overall F_{SypH}, obtained in the presence of NH_4Cl to de-quench all SypH molecules, similar decrease was observed (Fig. S6B–C). The ΔF decrease is not responsible for reduction of $Rate_{decay}$ in $Actb^{-/-}$ or $Actg1^{-/-}$ boutons, because $Train_{2s}$ in control induced a similarly small ΔF, but a $Rate_{decay}$ similar to that by $Train_{10s}$ in control (Fig. 6E–G), consistent with the general observation that exocytosis decrease does not slow endocytosis (Wu et al., 2014a).

The decrease of ΔF at $Actb^{-/-}$ or $Actg1^{-/-}$ boutons (Fig. 6G) is consistent with the slowdown of the RRP replenishment observed at $Actb^{-/-}$ or $Actg1^{-/-}$ calyces (Fig. 5D–G). ΔF decrease after a 10 s train at 20 Hz at hippocampal boutons (Fig. 6G) was larger than that at calyces after a 2 s train at 100 Hz (Fig. 3F). This difference could be due to different synapse types, as calyces experience much higher frequency of action potentials than hippocampal synapses and thus might have more robust mechanism to supply vesicles during repeated stimulation (Borst and Soria van Hoeve, 2012). Different recording conditions, the whole-cell patch-clamp capacitance recording at calyces versus extracellular stimulation with SypH imaging at hippocampal boutons, might also contribute to the difference. In addition, it might be in part due to different stimulation frequencies, because as we increased the 10 s train frequency from 20 to 80 Hz, ΔF (normalized to baseline F_{SypH}) induced in $Actb^{-/-}$ and control hippocampal boutons was 44 ± 3% (n = 5) and 88 ± 7% (n = 4), respectively (Fig. 6J). The decrease of ΔF (to ~50% of control) after the 80 Hz train (Fig. 6J) was smaller than that (to ~32% of control) after the 20 Hz train (Fig. 6G), but closer to that observed after a 2 s train of APe at 100 Hz at calyces (Fig. 3F).

Actin polymerization is needed for endocytosis

To exclude off-target effects of knockout, we transfected β-actin or γ-actin in $Actb^{-/-}$ or $Actg1^{-/-}$ boutons, respectively, to rescue knockout (transfection of β- or γ-actin, together with SypH and Cre-mCherry plasmids in $Actb^{LoxP/LoxP}$ or $Actg1^{LoxP/LoxP}$ cultures, respectively). In β-actin (Fig. 7A–B, n = 6 experiments, 3 mice) or γ-actin (Fig. 7C–D, n = 6, 3 mice) rescued boutons, $Train_{10s}$ induced a ΔF, a decay τ and a $Rate_{decay}$ similar to control boutons, confirming that the reduced $Rate_{decay}$ in $Actb^{-/-}$ (or $Actg1^{-/-}$) boutons is due to β-actin (or γ-actin) knockout.

Partial block of endocytosis by β- or γ-actin knockout suggests that both β- and γ-actin are needed for endocytosis. Partial reduction of β-actin to 55 ± 5% of control (n = 4, Fig. 6C) at 2 days after 4-OH-tamoxifen application to hippocampal cultures from $Cre\text{-}ER^{TM}$;$Actb^{LoxP/LoxP}$ mice was insufficient to inhibit endocytosis (Fig. S7A–B), suggesting that >45% reduction of β-actin is needed to inhibit endocytosis. Endocytosis was not inhibited when Cre was transfected to the $Actb^{LoxP/+}$;$Actg1^{LoxP/+}$ hippocampal culture to delete one allele of *Actb* and *Actg1* gene (Fig. S7C–D). Transfection of γ-actin to $Actb^{-/-}$ boutons (Fig. 7A–B) or β-actin to $Actg1^{-/-}$ boutons (Fig. 7C–D) rescued endocytosis to control, suggesting that actin amount is more important than specific actin isoform. Since overexpression extent was not quantified, we could not exclude the possibility that more γ-

actin than β-actin is needed to rescue endocytosis in Actb1$^{-/-}$ boutons (and vice versa). It remains possible that endogenous β- and γ-actin with a proper ratio are more efficient than the same amount of a single actin isoform.

Polymerized F-actin is known to exert mechanical forces (Blanchoin et al., 2014). To determine whether actin polymerization is needed for endocytosis, we transfected β-actin(G13R), an actin polymerization deficient mutant (Posern et al., 2002), in Actb$^{-/-}$ boutons (transfection of β-actin(G13R), SypH and Cre-mCherry plasmids in Actb$^{LoxP/LoxP}$ cultures). In these β-actin(G13R) rescued boutons, ΔF and $Rate_{decay}$ after $Train_{10s}$ were not rescued, but were similar to those obtained in Actb$^{-/-}$ boutons (Fig. 7E, F, n = 8, 3 mice), suggesting that actin polymerization is needed for endocytosis.

Electron microscopy at hippocampal synapses

We performed electron microscopy to examine ultrastructural changes in Cre-ER^{TM};Actb$^{LoxP/LoxP}$ hippocampal cultures at 4 days after 4-OH-tamoxifen treatment (TM4d-Actb$^{-/-}$ culture), which reduced β-actin to 13 ± 7% of control (Fig. 6C). Horseradish peroxidase (HRP, 5 mg/ml) was added to the bath for assay of vesicular uptake. In samples fixed in resting conditions, HRP-positive [HRP(+)] vesicles were minimal; most vesicles were HRP-negative [HRP(−)]; the number of HRP(+) and HRP(−) vesicles and their sum per μm^2 of synaptic cross section were similar in both control and TM4d-Actb$^{-/-}$ cultures (Fig. 8A–B). To examine endocytosis, we applied 90 mM KCl together with HRP for 1.5 min, and fixed samples at 0, 3 and 10 min after the end of the application of KCl and HRP. In control boutons, compared to the resting condition, HRP(+) vesicles increased from time 0 to 10 min after KCl, reflecting vesicle endocytosis; HRP(−) vesicles decreased at time 0 due to vesicle depletion by exocytosis, then increased from time 0 to 10 min, which is due to endocytosis that may not necessarily take up sufficient HRP to become HRP(+) (for detail, see Wu et al., 2014b); accordingly, the sum of HRP(+) and HRP(−) vesicles decreased, then increased, reflecting vesicle depletion and subsequent replenishment by endocytosis (Fig. 8A–B). Vesicle number did not return to baseline at 10 min after KCl (Fig. 8B), suggesting that endocytosis continues for > 10 min. These results are consistent with a recent work (Wu et al., 2014b).

Compared to control boutons, HRP(+) vesicles, HRP(−) vesicles, and their sum were significantly reduced at each time point after KCl in TM4d-Actb$^{-/-}$ boutons (Fig. 8A–B). Corroborating with results obtained with SypH imaging (Fig. 6), these decreases reflected inhibition of endocytosis, because exocytosis induced by 1.5 min KCl application was not decreased significantly in TM4d-Actb$^{-/-}$ boutons (Fig. S8). This insignificant reduction of exocytosis (Fig. S8) may be due to prolonged KCl application that may deplete a large fraction of vesicles in nerve terminals despite a slower vesicle mobilization observed in Actb$^{-/-}$ nerve terminals (Fig. 5D–G).

In control boutons, we observed HRP(+) bulk endosomes, defined as vesicles with a diameter > 80 nm or with a cross section area more than that of a 80 nm vesicle (~0.005 μm^2). Bulk endosome area increased at time 0, then decreased at 3 and 10 min (Fig. 8A, C), suggesting generation of bulk endosomes and subsequent conversion to vesicles (see also Wu et al., 2014b). Similar trends were observed in TM4d-Actb$^{-/-}$ boutons, but at a

significantly lower frequency (Fig. 8A, C), suggesting inhibition of bulk endocytosis by β-actin knockout, analogous to results obtained at calyces (Fig. 4).

In control boutons, compared to the resting condition, the number of pits, defined as having a height >15 nm, a base of 20–120 nm, and a height/base ratio >0.15, increased after KCl application. The pit frequency reached the peak at 3–10 min later (Fig. 8D–E), likely because endocytosis continued for > 10 min after KCl (Fig. 8A–C) (Wu et al., 2014b). In TM4d-Actb$^{-/-}$ boutons, the pit number after KCl was much lower than control boutons at every time point measured (Fig. 8D–E). The pit could be shallow or deep, or Ω-shape (Fig. 8D). We did not further discriminate these different shapes, because their frequency is too low for reliable quantification. The observed decrease of pits (Fig. 8E) could in principle be due to facilitation of fission or inhibition of pit generation. Since actin knockout inhibited SypH endocytosis (Figs. 6–7) and the number of endocytosed vesicles (Fig. 8A–C), but not the rate of fission pore closure during bulk endocytosis (Fig. 4C–D), the reduced pit number reflected inhibition of pit generation. These results suggest that actin is involved in endocytic pit formation.

Discussion

We found that β- or γ-actin knockout inhibited slow and rapid endocytosis induced by various stimulation protocols at 22–37°C (Figs. 1–3), reduced the frequency of DCSs that reflect bulk endocytosis (Fig. 4), and abolished endocytosis overshoot (Fig. 5) at calyces. β- or γ-actin knockout inhibited slow endocytosis at 22–37°C, and reduced HRP(+) synaptic vesicles and bulk endosomes at hippocampal synapses (Figs. 6–8). These results suggest that actin is crucial for rapid, slow, bulk and overshoot endocytosis in calyceal and hippocampal synapses. An actin mutant with a defect in polymerization could not rescue endocytosis in actin knockout boutons (Fig. 7), suggesting that polymerized F-actin, known to exert mechanical forces (Blanchoin et al., 2014), may provide force to mediate endocytosis. Actin knockout did not affect the rate of fission pore closure during bulk endocytosis at calyces (Fig. 4), but reduced membrane pit formation at hippocampal synapses (Fig. 8), suggesting that F-actin may exert mechanical force to bend membrane and thus to generate membrane pits. We also found that β- or γ-actin facilitates RRP replenishment (Fig. 5), most likely due to their role in endocytosis that facilitates active zone clearance. In summary, by performing genetic knockout and mutation, capacitance recordings, fission pore conductance measurements, pHluorin imaging, and electron microscopy, we found that actin is a key player for all kinetically distinguishable forms of endocytosis, and actin polymerization may provide mechanical force to bend membrane during endocytosis and facilitate the RRP replenishment.

Previous studies using actin-directed drugs yielded controversial results regarding whether actin plays a crucial role for all forms of endocytosis or a regulatory role for a specific form at a specific synapse (see Introduction). The controversy might be due to many factors, such as the drugs' off-target effects, their potentially differential access to different actin pools or different forms of endocytosis at various types of synapses *in vivo*, and/or the use of a single actin blocker at a single dose. The knockout approach we used avoided these potential pitfalls and produced consistent block of four forms of endocytosis detected with three

different techniques (capacitance measurements, SypH imaging and electron microscopy) in two synapse preparations, which allowed us to establish actin as an essential player for various forms of synaptic vesicle endocytosis. While we emphasize the knockout approach, the drug approach is sometimes advantageous, because it can produce results rapidly and does not have the compensatory effect that the knockout approach has to exclude.

Studies in non-neuronal mammalian cells using actin blockers also reach different conclusion as to whether actin is involved in endocytosis and at which step it is involved (Boulant et al., 2011; Ferguson et al., 2009; Merrifield et al., 2005; Saffarian et al., 2009; Yao et al., 2013; Yarar et al., 2005). Although a study explains this conflict by suggesting that actin dynamics is only needed on surfaces under tension (Boulant et al., 2011), differential access to different pools of actin in different *in vivo* conditions (including different surface tension) by actin blockers may provide an alternative explanation (Bleckert et al., 2012). We therefore suggest re-examination with knockout approach. It is likely that our finding of a universal role of actin in various forms of endocytosis may apply to non-neuronal cells, given that many aspects of synaptic vesicle endocytosis and non-neuronal vesicle endocytosis are conserved (Saheki and De Camilli, 2012).

It has been proposed that actin may participate in membrane invagination, coated pit formation, or fission at non-neuronal cells (Boulant et al., 2011; Ferguson et al., 2009; Merrifield et al., 2005; Saffarian et al., 2009; Yao et al., 2013; Yarar et al., 2005). At which step actin acts on synaptic vesicle endocytosis was unclear. Measurements of fission pore conductance and electron microscopy (Figs. 4, 8) suggest that polymerized actin is involved in generating membrane pits. It would be of great interest in the future to study how F-actin interacts with F-actin-related proteins and other endocytic proteins to generate such a pulling force.

Experimental Procedures

Animals

Animal care and use were carried out according to NIH guidelines and were approved by the NIH Animal Care and Use Committee. $Actb^{LoxP/LoxP}$ and $Actg1^{LoxP/LoxP}$ mice, generated as described previously (Perrin et al., 2010; Sonnemann et al., 2006), were obtained by homozygous breeding using standard mouse husbandry procedures. $Krox20^{Cre}$ mouse was generated as described previously (Voiculescu et al., 2000). To obtain $Krox20^{Cre/+}$;$Actb^{LoxP/LoxP}$ mice, we crossed $Krox20^{Cre/+}$ mice with $Actb^{LoxP/LoxP}$ mice and obtained the expected 50% Cre-positive and $Actb^{LoxP/+}$ offspring. By further crossing $Krox20^{Cre/+}$;$Actb^{LoxP/+}$ mouse line with $Actb^{LoxP/LoxP}$ mouse line, we got the expected 25% $Krox20^{Cre/+}$;$Actb^{LoxP/LoxP}$ offspring mice, which were identified with PCR-based genotyping and used for experiments. The Cre-negative $Actb^{LoxP/LoxP}$ littermates were used as control mice. Similar breeding strategy was used to generate $Krox20^{Cre/+}$;$Actg1^{LoxP/LoxP}$ mice. *CAGGCre-EM*^{TM} mice were obtained from Jackson Lab. Its Cre efficiency induced by tamoxifen reaches 90% in cultured cells (Hayashi and McMahon, 2002). Cre-ER^{TM};$Actb^{LoxP/LoxP}$ mice were generated by crossing *CAGGCre-EM*^{TM} mice with $Actb^{LoxP/LoxP}$ mice.

Slice preparation, capacitance recordings and solutions

Parasagittal brainstem slices (200 μm thick) containing the MNTB were prepared from 7–14 days old male or female mice using a vibratome (Wu et al., 2009). Whole-cell capacitance measurements were made with the EPC-9 amplifier with a software lock-in amplifier (1000 Hz sine wave, peak-to-peak voltage ≤ 60 mV, HEKA, Lambrecht, Germany). We pharmacologically isolated presynaptic Ca^{2+} currents with a bath solution (~22–24°C or 34–37°C when mentioned) containing (in mM): 105 NaCl, 20 TEA-Cl, 2.5 KCl, 1 $MgCl_2$, 2 $CaCl_2$, 25 $NaHCO_3$, 1.25 NaH_2PO_4, 25 glucose, 0.4 ascorbic acid, 3 *myo*-inositol, 2 sodium pyruvate, 0.001 tetrodotoxin (TTX), 0.1 3,4-diaminopyridine, pH 7.4 when bubbled with 95% O_2 and 5% CO_2. The presynaptic pipette contained (in mM): 125 Cs-gluconate, 20 CsCl, 4 MgATP, 10 Na_2-phosphocreatine, 0.3 GTP, 10 HEPES, 0.05 BAPTA, pH 7.2, adjusted with CsOH. If not mentioned otherwise, all reagents were purchased from Sigma (St. Louis, MO).

In temperature experiments, the continuously flowing solution reached the slice chamber via a tube, which was heated to ~40–42°C right (at ~10–15 cm) before the solution reached the chamber. With a flow rate of ~2.5 ml/min, the chamber temperature was maintained at 34–37°C, as confirmed with a thermometer. Slices were at 34–37°C for ~15–20 min before patching.

Hippocampal culture

Mouse hippocampal culture was prepared as described previously (Sankaranarayanan and Ryan, 2000; Sun et al., 2010). Hippocampal CA1-CA3 regions from P0 mice were dissected, dissociated, and plated on Poly-D-lysince treated coverslips. Cells were maintained at 37°C in a 5% CO_2 humidified incubator with a culture medium consisting of MEM (Invitrogen, Carlsbad, CA), 0.5% glucose, 0.1 g/l bovine transferrin (Calbiochem, La Jolla, CA), 0.3 g/l glutamine, 10% fetal bovine serum (Invitrogen, Carlsbad, CA), 2% B-27 (Invitrogen, Carlsbad, CA), and 3 μM cytosine β-D-arabinofuranoside. On 5–7 days after plating, neurons were transfected with plasmids using Lipofectamine LTX (Invitrogen, Carlsbad, CA).

Hippocampal cultures were transfected with a plasmid containing SypH alone (control) or with L309 plasmid containing Cre-mcherry. A nuclear localization sequence was tagged at the N-terminal of Cre, which was then cloned into L309 vector (a gift from Dr. Thomas Sudhof and Zhiping Pang, Stanford university) via BamHI and EcoRI sites. Plasmids containing β-actin or γ-actin were purchased from Origene (Rockville, MD). Site-directed mutagenesis was performed on β-actin to generate β-actin(G13R) mutant. For actin rescue, we transfected β- or γ-actin plasmid along with SypH and L309 plasmid containing Cre-mcherry. After transfection, neurons were maintained at 37°C in a 5% CO2 humidified incubator for another 8–12 days before experiments.

Action potential was evoked by a 1 ms pulse (20 mA) through a platinum electrode. The bath solution contained (in mM): 119 NaCl, 2.5 KCl, 2 $CaCl_2$, 2 $MgCl_2$, 25 HEPES (buffered to pH 7.4), 30 glucose, 0.01 6-cyano-7-nitroquinoxaline-2, 3-dione (CNQX), and 0.05 D, L-2-amino-5-phosphonovaleric acid (AP-5). In temperature experiments, we heated

the culture chamber using a temperature controller (TC344B, Warner Instruments, Hamden, CT). Imaging was performed after the culture was at 34–37°C for 15–30 min. The temperature was verified with another small thermometer (BAT-7001H, Physitemp Instruments, Clifton, NJ) in the chamber. SypH images were acquired at 1 Hz using Nikon A1 confocal microscope (60X, 1.4 NA), and analyzed with Nikon software. All boutons showing fluorescence increases were analyzed (region of interest: 2 μm × 2 μm). Each data group was obtained from at least three batches of cultures.

Lentivirus Production

Cre with nuclear localization sequence at the N-terminus was inserted between BamHI and EcoRI restriction enzyme digestion sites in L309 lentiviral vector to generate L309-Cre plasmid. L309-Cre, along with two other viral envelope protein encoding vectors, VSVg and delta 8.9, were co-transfected into HEK293T cells using calcium phosphate (BD Bioscience, San Jose, CA). Three to four days after transfection, the supernatant was collected, filtered to remove cell particles, centrifuged at 20,000 rpm for two hours to concentrate the virus, and dissolved in 100 μl PBS per 30 ml supernatant.

Immunohistochemistry and Western blot

For immunohistochemistry, P9 mice were anesthetized using Nembutal and transcardially perfused with 4% paraformaldehyde (Electron Microscopy Sciences, Hatfield, PA). The brain was post-fixed in 4% paraformaldehyde overnight and infiltrated with 30% sucrose for another 48 hrs. OCT (Electron Microscopy Sciences) embedded brain was sectioned using cryostat (Leica CM3050S) at 30 μm thickness. Slices were treated with cold methanol at −20°C for 10 min, and target proteins at calyces were identified using a guinea pig antibody against $vGluT_1$ (1:5,000; Millipore, Billerica, MA) and FITC-conjugated β-actin antibody (1:75; Abcam, Cambridge, MA) or Alexa 568 conjugated γ-actin antibody (mAB1-37; 1:50) (Perrin et al., 2010). ZsGreen was recognized with a rabbit anti zsGreen antibody (Clontech, 1:100). Dylight-488 conjugated donkey anti-guinea pig antibody (1:200; Jackson ImmunoResearch Laboratories, West Grove, PA) or Rhodamine-red-X conjugated donkey anti-guinea pig antibody (1:200; Jackson ImmunoResearch Laboratories, West Grove, PA) was used as secondary antibodies. Images were collected by Nikon A1 confocal microscopy (60X, 1.4 NA).

For Western blot, neurons were washed three times with ice-cold PBS. Cell lysates were prepared in the modified RIPA buffer containing protease inhibitors (Thermo Scientific, Rockford, IL). Equal amounts of proteins, determined by BCA protein assay (Thermo Scientific), were loaded onto SDS-PAGE gel and immunoblotted using antibodies against β-actin (1: 1000, Abcam, Cambridge, MA), γ-actin (mAB1-37; 1:500), AP-2 (1:100, Thermo Scientific), clathrin heavy chain (1:1,000, BD Bioscience, San Jose, CA), dynamin (1:1,000; BD Bioscience) and GAPDH (1:2,000; Sigma).

Data collection and measurements of τ, $Rate_{decay}$, and DCS

The statistical test was t-test. Means were presented as ± s.e.m. Calyx capacitance was measured within 10 min after break-in to avoid rundown (Wu et al., 2009). The τ was measured from exponential fit. $Rate_{decay}$ at calyces was measured between 0.5 – 4 s after

$depol_{20ms}$ or 20 APe at 100 Hz that induced slow endocytosis, but between 0.5 – 1.5 s after $depol_{20msX10}$ or 200 APe at 100 Hz that induced rapid endocytosis. The first 0.5 s trace was not used to avoid capacitance artifact contamination (Wu et al., 2005; Yamashita et al., 2005). We used $depol_{20msX10}$ to induce rapid endocytosis, because the $Rate_{decay}$ after $depol_{20msX10}$ reflected mostly (~80%) the rapid component of endocytosis (Sun et al., 2010; Wu et al., 2009). For SypH signal in hippocampal cultures, the $Rate_{decay}$ was measured from F_{SypH} in the first 4–10 s after stimulation.

Measurements of DCSs and G_p are described previously (Wu and Wu, 2007). Briefly, to detect DCSs, capacitance traces were low-pass filtered at 30 Hz, and differentiated. The differentiation was calculated as the difference between capacitance values of two neighboring samples with an interval of 1 ms. A DCS was identified when the rate of decay was >50 fF/100 ms in the differentiated trace, the DCS size was > 20 fF in the filtered trace, and the measured series conductance and membrane conductance did not change in parallel with the DCS.

Electron microscopy

Hippocampal cultures were fixed with 4% glutaraldehyde (freshly prepared, Electron microscopy sciences, Hatfield, PA) in 0.1 N Na-cacodylate buffer solution containing for at least one hour at 22–24°C, and stored in 4°C refrigerator overnight. The next day, cultures were washed with 0.1 N cacodylate buffer, and treated with 1% OsO4 in cacodylate buffer for 1 hr on ice, and 0.25% uranyl acetate in acetate buffer at pH 5.0 overnight at 4°C, dehydrated with ethanol, and embedded in epoxy resin. Thin sections were counterstained with uranyl acetate and lead citrate then examined in a JEOL200CX TEM. Images were collected with a CCD digital camera system (XR-100 from AMT, Danvers, MA) at a primary magnification of 10,000–20,000X. Synapses were selected based on the structural specialization including synaptic vesicle clustering, synaptic cleft and the postsynaptic density. Each group of data was taken from 40–100 synaptic profiles from 4–8 mice.

Supplementary Material

Refer to Web version on PubMed Central for supplementary material.

Acknowledgments

This work was supported by the National Institute of Neurological Disorders and Stroke Intramural Research Program in USA, and a fellowship program from Korea Research Institute of Bioscience and Biotechnology in Republic of Korea. We thank Dr. Yongling Zhu (Northwestern University, Chicago) for providing synaptophysin-pHluorin2X plasmid, Drs. Zhiping Pang and Thomas C. Sudhof for the gift of L309 plasmid, and Dr. Ralf Schneggenburger (EPFL, Switzerland) for shipping $krox20^{Cre}$ mice.

Reference List

Betz WJ, Henkel AW. Okadaic acid disrupts clusters of synaptic vesicles in frog motor nerve terminals. J Cell Biol. 1994; 124:843–854. [PubMed: 8120104]

Blanchoin L, Boujemaa-Paterski R, Sykes C, Plastino J. Actin dynamics, architecture, and mechanics in cell motility. Physiol Rev. 2014; 94:235–263. [PubMed: 24382887]

Bleckert A, Photowala H, Alford S. Dual pools of actin at presynaptic terminals. J Neurophysiol. 2012; 107:3479–3492. [PubMed: 22457456]

Borst JG, Soria van Hoeve J. The calyx of held synapse: from model synapse to auditory relay. Annu Rev Physiol. 2012; 74:199–224. [PubMed: 22035348]

Boulant S, Kural C, Zeeh JC, Ubelmann F, Kirchhausen T. Actin dynamics counteract membrane tension during clathrin-mediated endocytosis. Nat Cell Biol. 2011; 13:1124–1131. [PubMed: 21841790]

Bourne J, Morgan JR, Pieribone VA. Actin polymerization regulates clathrin coat maturation during early stages of synaptic vesicle recycling at lamprey synapses. J Comp Neurol. 2006; 497:600–609. [PubMed: 16739194]

Cheever TR, Ervasti JM. Actin isoforms in neuronal development and function. Int Rev Cell Mol Biol. 2013; 301:157–213. [PubMed: 23317819]

Delvendahl I, Vyleta NP, von Gersdorff H, Hallermann S. Fast, Temperature-Sensitive and Clathrin-Independent Endocytosis at Central Synapses. Neuron. 2016; 90:492–498. [PubMed: 27146271]

Engqvist-Goldstein AE, Drubin DG. Actin assembly and endocytosis: from yeast to mammals. Annu Rev Cell Dev Biol. 2003; 19:287–332. [PubMed: 14570572]

Ferguson SM, Raimondi A, Paradise S, Shen H, Mesaki K, Ferguson A, Destaing O, Ko G, Takasaki J, Cremona O, O'Toole E, De Camilli P. Coordinated actions of actin and BAR proteins upstream of dynamin at endocytic clathrin-coated pits. Dev Cell. 2009; 17:811–822. [PubMed: 20059951]

Han Y, Kaeser PS, Sudhof TC, Schneggenburger R. RIM determines Ca(2)+ channel density and vesicle docking at the presynaptic active zone. Neuron. 2011; 69:304–316. [PubMed: 21262468]

Hayashi S, McMahon AP. Efficient recombination in diverse tissues by a tamoxifen-inducible form of Cre: a tool for temporally regulated gene activation/inactivation in the mouse. Dev Biol. 2002; 244:305–318. [PubMed: 11944939]

He L, Xue L, Xu J, McNeil BD, Bai L, Melicoff E, Adachi R, Wu LG. Compound vesicle fusion increases quantal size and potentiates synaptic transmission. Nature. 2009; 459:93–97. [PubMed: 19279571]

Herman IM. Actin isoforms. Curr Opin Cell Biol. 1993; 5:48–55. [PubMed: 8448030]

Holt M, Cooke A, Wu MM, Lagnado L. Bulk membrane retrieval in the synaptic terminal of retinal bipolar cells. J Neurosci. 2003; 23:1329–1339. [PubMed: 12598621]

Hua Y, Sinha R, Thiel CS, Schmidt R, Hüve J, Martens H, Hell SW, Egner A, Klingauf J. A readily retrievable pool of synaptic vesicles. Nat Neurosci. 2011a; 14:833–839. [PubMed: 21666673]

Hua Z, Leal-Ortiz S, Foss SM, Waites CL, Garner CC, Voglmaier SM, Edwards RH. v-SNARE composition distinguishes synaptic vesicle pools. Neuron. 2011b; 71:474–487. [PubMed: 21835344]

Job C, Lagnado L. Calcium and protein kinase C regulate the actin cytoskeleton in the synaptic terminal of retinal bipolar cells. J Cell Biol. 1998; 143:1661–1672. [PubMed: 9852158]

Li Z, Murthy VN. Visualizing postendocytic traffic of synaptic vesicles at hippocampal synapses. Neuron. 2001; 31:593–605. [PubMed: 11545718]

Madisen L, Zwingman TA, Sunkin SM, Oh SW, Zariwala HA, Gu H, Ng LL, Palmiter RD, Hawrylycz MJ, Jones AR, Lein ES, Zeng H. A robust and high-throughput Cre reporting and characterization system for the whole mouse brain. Nat Neurosci. 2010; 13:133–140. [PubMed: 20023653]

Merrifield CJ, Perrais D, Zenisek D. Coupling between clathrin-coated-pit invagination, cortactin recruitment, and membrane scission observed in live cells. Cell. 2005; 121:593–606. [PubMed: 15907472]

Micheva KD, Smith SJ. Strong effects of subphysiological temperature on the function and plasticity of mammalian presynaptic terminals. J Neurosci. 2005; 25:7481–7488. [PubMed: 16107635]

Neher E. What is Rate-Limiting during Sustained Synaptic Activity: Vesicle Supply or the Availability of Release Sites. Front Synaptic Neurosci. 2010; 2:144. [PubMed: 21423530]

Perrin BJ, Sonnemann KJ, Ervasti JM. beta-actin and gamma-actin are each dispensable for auditory hair cell development but required for Stereocilia maintenance. PLoS Genet. 2010; 6:e1001158. [PubMed: 20976199]

Posern G, Sotiropoulos A, Treisman R. Mutant actins demonstrate a role for unpolymerized actin in control of transcription by serum response factor. Mol Biol Cell. 2002; 13:4167–4178. [PubMed: 12475943]

Renden R, von Gersdorff H. Synaptic vesicle endocytosis at a CNS nerve terminal: faster kinetics at physiological temperatures and increased endocytotic capacity during maturation. J Neurophysiol. 2007; 98:3349–3359. [PubMed: 17942618]

Richards DA, Rizzoli SO, Betz WJ. Effects of wortmannin and latrunculin A on slow endocytosis at the frog neuromuscular junction. J Physiol. 2004; 557:77–91. [PubMed: 15004214]

Saffarian S, Cocucci E, Kirchhausen T. Distinct dynamics of endocytic clathrin-coated pits and coated plaques. PLoS Biol. 2009; 7:e1000191. [PubMed: 19809571]

Saheki Y, De Camilli P. Synaptic vesicle endocytosis. Cold Spring Harb Perspect Biol. 2012; 4:a005645. [PubMed: 22763746]

Sakaba T, Neher E. Involvement of actin polymerization in vesicle recruitment at the calyx of Held synapse. J Neurosci. 2003; 23:837–846. [PubMed: 12574412]

Sankaranarayanan S, Atluri PP, Ryan TA. Actin has a molecular scaffolding, not propulsive, role in presynaptic function. Nat Neurosci. 2003; 6:127–135. [PubMed: 12536209]

Sankaranarayanan S, Ryan TA. Real-time measurements of vesicle-SNARE recycling in synapses of the central nervous system. Nat Cell Biol. 2000; 2:197–204. [PubMed: 10783237]

Shawlot W, Deng JM, Fohn LE, Behringer RR. Restricted beta-galactosidase expression of a hygromycin-lacZ gene targeted to the beta-actin locus and embryonic lethality of beta-actin mutant mice. Transgenic Res. 1998; 7:95–103. [PubMed: 9608737]

Shmerling D, Danzer CP, Mao X, Boisclair J, Haffner M, Lemaistre M, Schuler V, Kaeslin E, Korn R, Bürki K, Ledermann B, Kinzel B, Muller M. Strong and ubiquitous expression of transgenes targeted into the beta-actin locus by Cre/lox cassette replacement. Genesis. 2005; 42:229–235. [PubMed: 16028230]

Shupliakov O, Bloom O, Gustafsson JS, Kjaerulff O, Low P, Tomilin N, Pieribone VA, Greengard P, Brodin L. Impaired recycling of synaptic vesicles after acute perturbation of the presynaptic actin cytoskeleton. Proc Natl Acad Sci U S A. 2002; 99:14476–14481. [PubMed: 12381791]

Sonnemann KJ, Fitzsimons DP, Patel JR, Liu Y, Schneider MF, Moss RL, Ervasti JM. Cytoplasmic gamma-actin is not required for skeletal muscle development but its absence leads to a progressive myopathy. Dev Cell. 2006; 11:387–397. [PubMed: 16950128]

Sun JY, Wu LG. Fast kinetics of exocytosis revealed by simultaneous measurements of presynaptic capacitance and postsynatpic currents at a central synapse. Neuron. 2001; 30:171–182. [PubMed: 11343653]

Sun T, Wu XS, Xu J, McNeil BD, Pang ZP, Yang W, Bai L, Qadri S, Molkentin JD, Yue DT, Wu LG. The role of calcium/calmodulin-activated calcineurin in rapid and slow endocytosis at central synapses. J Neurosci. 2010; 30:11838–11847. [PubMed: 20810903]

Voiculescu O, Charnay P, Schneider-Maunoury S. Expression pattern of a Krox-20/Cre knock-in allele in the developing hindbrain, bones, and peripheral nervous system. Genesis. 2000; 26:123–126. [PubMed: 10686605]

Watanabe S, Trimbuch T, Camacho-Perez M, Rost BR, Brokowski B, Sohl-Kielczynski B, Felies A, Davis MW, Rosenmund C, Jorgensen EM. Clathrin regenerates synaptic vesicles from endosomes. Nature. 2014; 515:228–233. [PubMed: 25296249]

Wu LG, Hamid E, Shin W, Chiang HC. Exocytosis and endocytosis: modes, functions, and coupling mechanisms. Annu Rev Physiol. 2014a; 76:301–331. [PubMed: 24274740]

Wu W, Wu LG. Rapid bulk endocytosis and its kinetics of fission pore closure at a central synapse. Proc Natl Acad Sci U S A. 2007; 104:10234–10239. [PubMed: 17551019]

Wu W, Xu J, Wu XS, Wu LG. Activity-dependent acceleration of endocytosis at a central synapse. J Neurosci. 2005; 25:11676–11683. [PubMed: 16354926]

Wu XS, McNeil BD, Xu J, Fan J, Xue L, Melicoff E, Adachi R, Bai L, Wu LG. Ca(2+) and calmodulin initiate all forms of endocytosis during depolarization at a nerve terminal. Nat Neurosci. 2009; 12:1003–1010. [PubMed: 19633667]

Wu Y, O'Toole ET, Girard M, Ritter B, Messa M, Liu X, McPherson PS, Ferguson SM, De Camilli P. A dynamin 1-, dynamin 3- and clathrin-independent pathway of synaptic vesicle recycling mediated by bulk endocytosis. Elife. 2014b; 3:e01621. [PubMed: 24963135]

Xue L, McNeil BD, Wu XS, Luo F, He L, Wu LG. A membrane pool retrieved via endocytosis overshoot at nerve terminals: a study of its retrieval mechanism and role. J Neurosci. 2012; 32:3398–3404. [PubMed: 22399762]

Yamashita T, Hige T, Takahashi T. Vesicle endocytosis requires dynamin-dependent GTP hydrolysis at a fast CNS synapse. Science. 2005; 307:124–127. [PubMed: 15637282]

Yao LH, Rao Y, Bang C, Kurilova S, Varga K, Wang CY, Weller BD, Cho W, Cheng J, Gong LW. Actin polymerization does not provide direct mechanical forces for vesicle fission during clathrin-mediated endocytosis. J Neurosci. 2013; 33:15793–15798. [PubMed: 24089486]

Yarar D, Waterman-Storer CM, Schmid SL. A dynamic actin cytoskeleton functions at multiple stages of clathrin-mediated endocytosis. Mol Biol Cell. 2005; 16:964–975. [PubMed: 15601897]

Zhu Y, Xu J, Heinemann SF. Two pathways of synaptic vesicle retrieval revealed by single-vesicle imaging. Neuron. 2009; 61:397–411. [PubMed: 19217377]

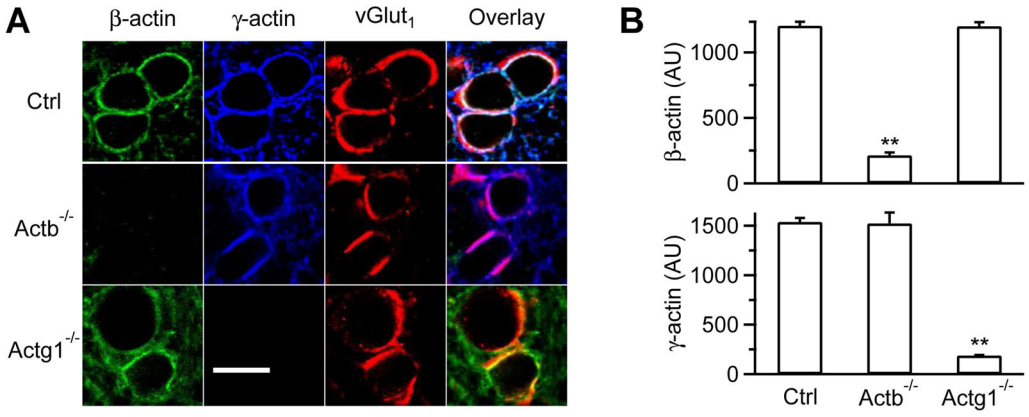

Figure 1. Actb$^{-/-}$ and Actg1$^{-/-}$ calyces

(A) Antibody staining of β-actin, γ-actin, and vGluT$_1$ in P9 control (Ctrl), Actb$^{-/-}$, and Actg1$^{-/-}$ calyces (images overlay in the right).

(B) β- and γ-actin staining intensity (mean + s.e.m., AU, arbitrary unit) in P7-10 Ctrl (54 calyces, 3 mice), Actb$^{-/-}$ (56 calyces, 3 mice), and Actg1$^{-/-}$ calyces (53 calyces, 3 mice). **: $p<0.01$ (t test, compared to Ctrl).

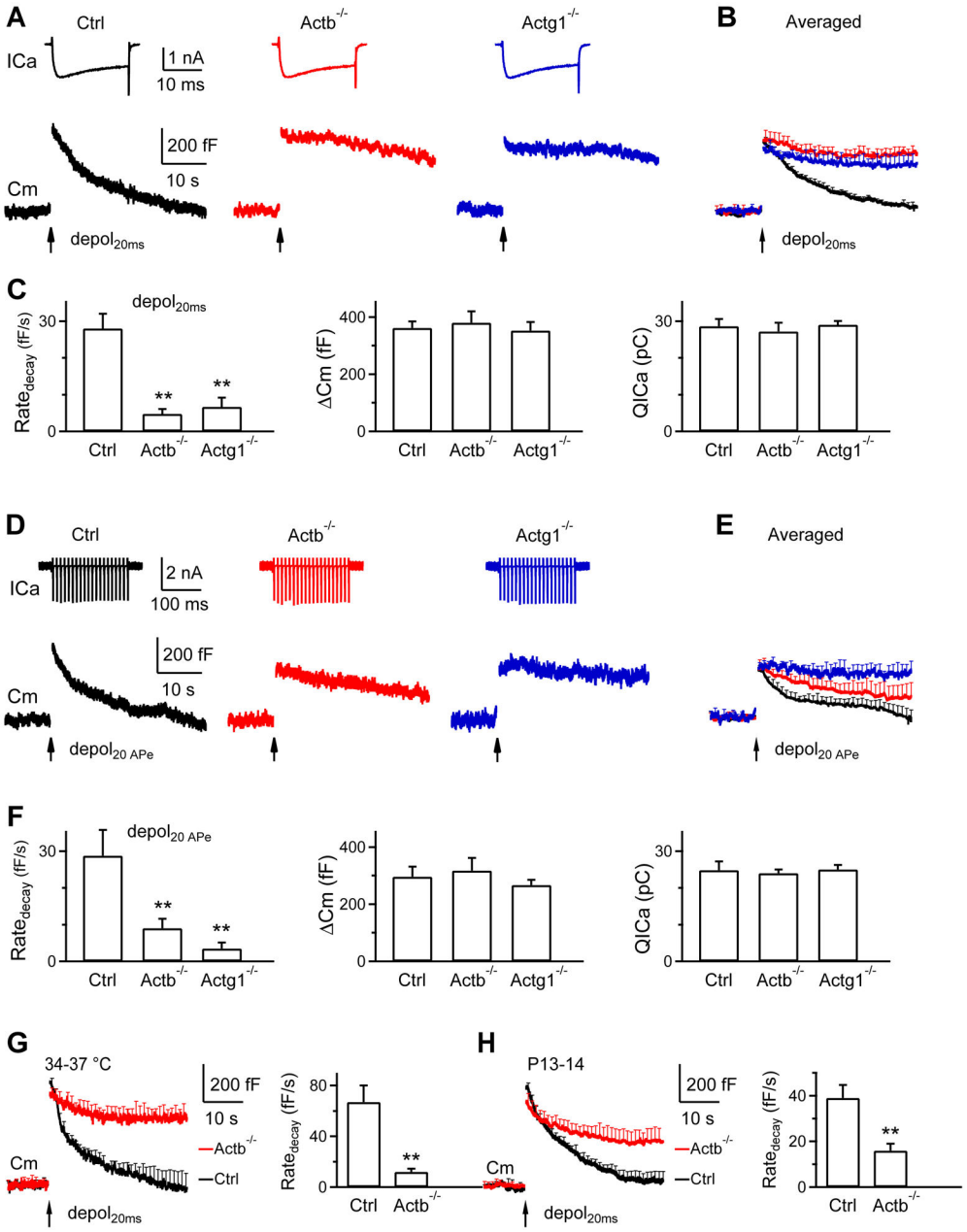

Figure 2. β- or γ-actin knockout inhibits slow endocytosis at calyces

(A–C) Sampled ICa and Cm (A), mean Cm traces (mean + s.e.m., B), and $Rate_{decay}$, ΔCm and QICa (mean + s.e.m., C) induced by $depol_{20ms}$ (arrow) from Ctrl (13 calyces, 13 mice, black), $Actb^{-/-}$ (12 calyces, 8 mice, red) and $Actg1^{-/-}$ (12 calyces, 9 mice, blue) calyces from P7-10 mice at 22–24°C. s.e.m. is plotted every 1 s. **, $p<0.01$ (t test, applies to other plots). The first 0.5 s Cm trace after $depol_{20ms}$, which may contain Cm artifacts, was not shown (applies to all Cm trace in Fig. 2).

(D–F) Similar to A-C, except that the stimulus was 20 APe at 100 Hz (P7-10, 22–24°C). Control, n = 7 calyces, 7 mice; $Actb^{-/-}$, n = 6 calyces, 6 mice; $Actg1^{-/-}$, n = 6 calyces, 6 mice.

(G) Cm traces and $Rate_{decay}$ (mean + s.e.m.) induced by $depol_{20ms}$ from Ctrl (8 calyces, 8 mice) and $Actb^{-/-}$ (8 calyces, 8 mice) calyces at 34–37°C (P7-10). **, $p<0.01$ (t test).
(H) Cm traces and $Rate_{decay}$ (mean + s.e.m.) induced by $depol_{20ms}$ from Ctrl (10 calyces, 9 mice) and $Actb^{-/-}$ (9 calyces, 9 mice) calyces in P13-14 mice (22–24°C). **, $p<0.01$ (t test).

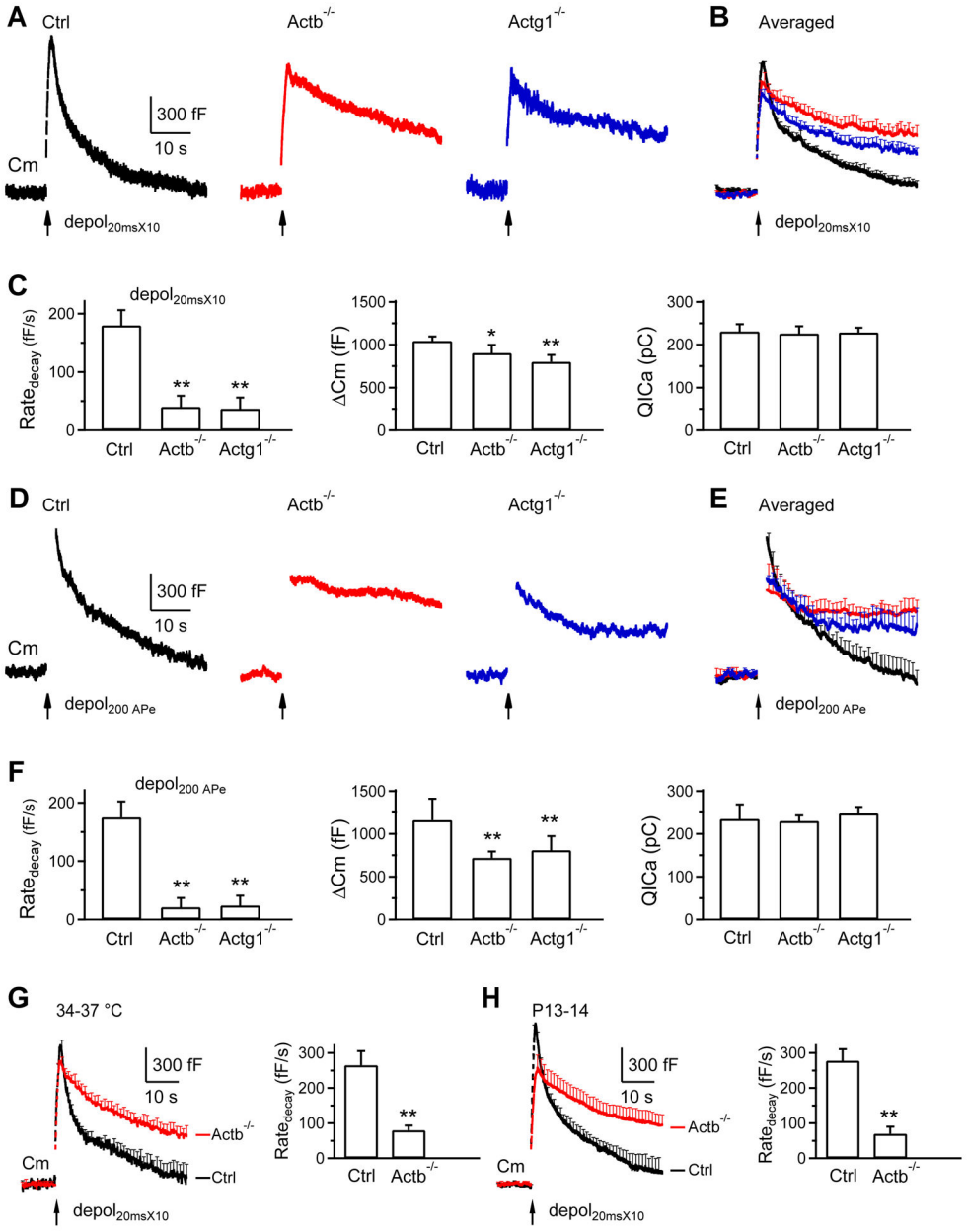

Figure 3. β- or γ-actin knockout inhibits rapid endocytosis at calyces

(A–H) Similar arrangements as Fig. 2A–H, respectively, except that the stimulus was $depol_{20msX10}$ (A–C, G–H) or 200 APe at 100 Hz (D–F). A–C: Ctrl, 13 calyces, 13 mice; $Actb^{-/-}$, 12 calyces, 8 mice; $Actg1^{-/-}$, 12 calyces, 9 mice (P7-10, 22–24°C). D–F: Ctrl, 7 calyces, 6 mice; $Actb^{-/-}$, 6 calyces, 5 mice; $Actg1^{-/-}$, 6 calyces, 5 mice (P7-10, 22–24°C). G: Ctrl, 8 calyces, 8 mice; $Actb^{-/-}$, 8 calyces, 8 mice (P7-10, 34–37°C). H: Ctrl, 10 calyces, 9 mice; $Actb^{-/-}$, 9 calyces, 9 mice (P13-14, 22–24°C). *, p<0.05; **, p<0.01 (t test).

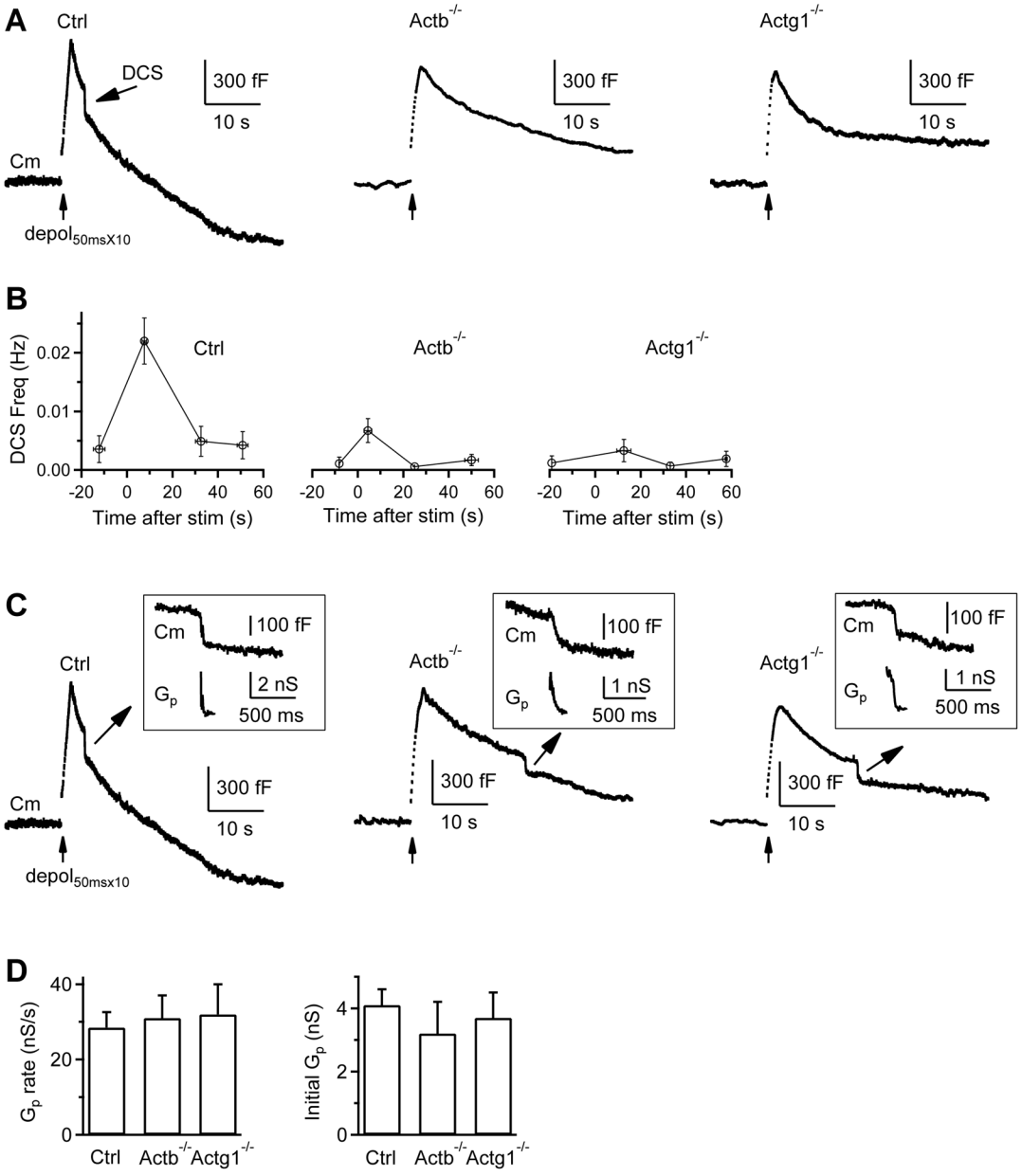

Figure 4. β- or γ-actin knockout inhibits bulk endocytosis and an endocytic step before fission pore closure

(A–B) Sampled Cm (A) and DCS frequency (B, mean ± s.e.m) induced by $depol_{50msX10}$ with 5.5 mM calcium in the bath from Ctrl (n = 24 calyces), $Actb^{-/-}$ (n = 29 calyces), and $Actg1^{-/-}$ (n = 18 calyces) calyces. The arrow points to a DCS in Ctrl (A, left). DCS frequency, binned every 20 s, is plotted versus time before and after $depol_{50msX10}$ (time 0). (C) Sampled Cm with a DCS and an accompanying G_p shown enlarged in the inset from a Ctrl, $Actb^{-/-}$, and $Actg1^{-/-}$ calyx. Ctrl trace is the same as the Ctrl trace in A. The stimulation was $depol_{50msX10}$ with 5.5 mM calcium in the bath (also applies to D).

(D) The mean (+s.e.m.) rate of G_p change and initial G_p during DCSs in control (43 DCSs), $Actb^{-/-}$ (15 DCSs), and $Actg1^{-/-}$ (9 DCSs) calyces. No statistical difference was observed ($p > 0.14$, t test).

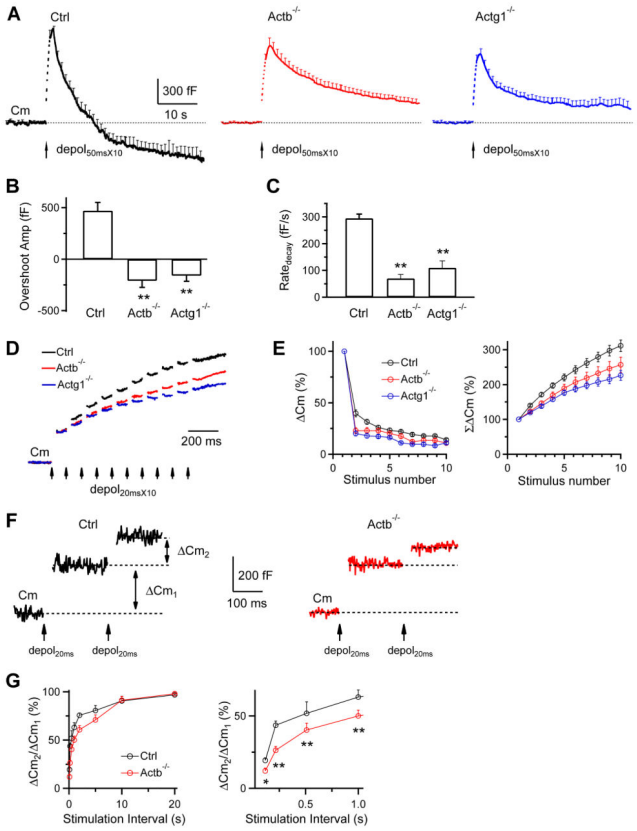

Figure 5. β-actin or γ-actin knockout inhibits endocytosis overshoot and the RRP replenishment

(A) Averaged Cm changes (mean + s.e.m.) induced by $depol_{50msX10}$ (arrow) from control (24 calyces), $Actb^{-/-}$ (29 calyces) and $Actg1^{-/-}$ (18 calyces) mice (bath: 5.5 mM calcium). Dotted line: baseline.

(B–C) The endocytosis overshoot amplitude (mean + s.e.m.) measured at 40 s after $depol_{50msX10}$ (B) and the $Rate_{decay}$ after $depol_{50msX10}$ (C) in control (n = 24), $Actb^{-/-}$ (n = 29) and $Actg1^{-/-}$ (n = 18) calyces (bath: 5.5 mM calcium). A positive value means an overshoot. **: p <0.01, t test.

(D) Sampled Cm induced by $depol_{20msX10}$ (each arrow: 1 $depol_{20ms}$) from Ctrl, $Actb^{-/-}$ and $Actg1^{-/-}$ calyces. The Cm jump induced by the first $depol_{20ms}$ was normalized for comparison. Bath: 2 mM calcium (applies to panel D–G)

(E) ΔCm (left) and the accumulated ΔCm (ΣΔCm, right) induced by each of the 10 $depol_{20ms}$ during $depol_{20msX10}$ in Ctrl (13 calyces), $Actb^{-/-}$ (12 calyces) and $Actg1^{-/-}$ (12 calyces) calyces. Data (mean ± s.e.m.) are normalized to the ΔCm induced by the 1st $depol_{20ms}$.

(F) Sampled Cm traces induced by a pair of $depol_{20ms}$ at an interval of 200 ms in a Ctrl and a $Actb^{-/-}$ calyx.

(G) Left: the ratio between the 2nd and the 1st ΔCm ($\Delta Cm_2/\Delta Cm_1$) during a pair of $depol_{20ms}$ plotted versus paired-pulse interval (each data point: 5–7 calyces). Right: same as in left, but plotting the interval between 0–1 s. *: p < 0.05; **: p < 0.01 (t test).

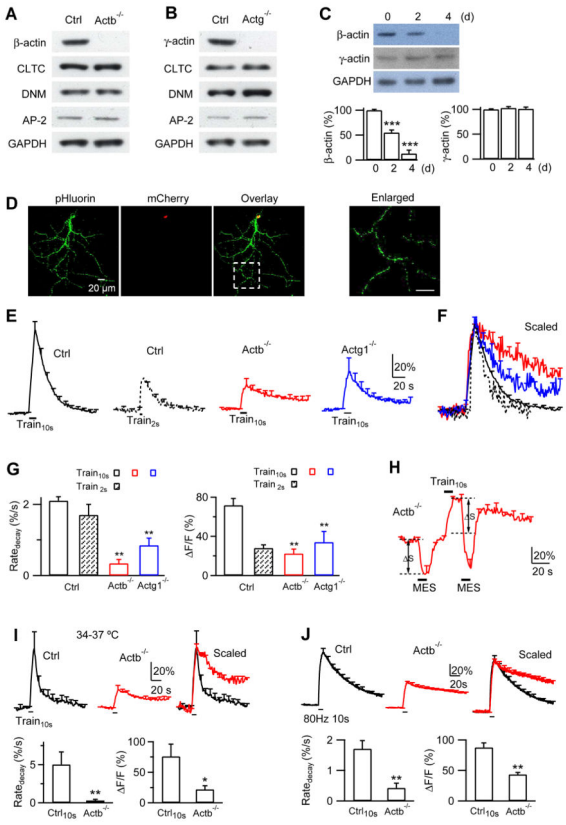

Figure 6. β- or γ-actin knockout inhibits endocytosis at hippocampal synapses

(A) Western blot of β-actin, AP-2, Clathrin heavy chain (CLT), dynamin (DMN) and GAPDH (Glyceraldehyde 3-phosphate dehydrogenase, loading control) from $Actb^{LoxP/LoxP}$ hippocampal cultures transfected with nothing (Ctrl) or with lentivirus containing a Cre enzyme ($Actb^{-/-}$).

(B) Similar to A, except from $Actg1^{LoxP/LoxP}$ cultures.

(C) Upper: western blot of β-actin, γ-actin and GAPDH from Cre-ER^{TM};$Actb^{LoxP/LoxP}$ culture at 0, 2 and 4 days (d) after addition of 4-OH-tamoxifen (1 μM).

Lower: β- (left) and γ-actin (right) western blot intensity from Cre-ER^{TM};$Actb^{LoxP/LoxP}$ culture at 0, 2 and 4 days after addition of 4-OH-tamoxifen (mean + s.e.m., normalized to day 0, n = 4). ***, $p < 0.001$ (ANOVA).

(D) SypH and mCherry images of a neuron transfected with SypH and a plasmid containing Cre-mCherry. mCherry is localized to nucleus (superimposed image), due to a nuclear localization sequence tagged at the Cre N-terminal. The box region is enlarged (right) to indicate a place for SypH imaging.

(E) F_{SypH} (mean + s.e.m.) induced by $Train_{10s}$ (left, n = 8 experiments) or $Train_{2s}$ (n = 5) in control boutons, and F_{SypH} induced by $Train_{10s}$ in $Actb^{-/-}$ boutons ($Actb^{LoxP/LoxP}$ boutons transfected with SypH and a Cre plasmid, n = 11) or in $Actg1^{-/-}$ boutons ($Actg1^{LoxP/LoxP}$ boutons transfected with SypH and a Cre plasmid, n = 10). F_{SypH} is normalized to baseline, s.e.m. is plotted every 10 s, temperature was 22–24°C (applies to Figs. 6–8 if not mentioned otherwise).

(F) Traces in E (same color coding) scaled to the same amplitude and superimposed. $Train_{2s}$ was aligned to the end of $Train_{10s}$.

(G) $Rate_{decay}$ and ΔF (mean + s.e.m.) induced by $Train_{10s}$ and $Train_{2s}$ in control boutons ($Train_{10s}$, n = 8; $Train_{2s}$, n = 5) and by $Train_{10s}$ in $Actb^{-/-}$ (n = 11) and $Actg1^{-/-}$ boutons (n = 10 experiments). ΔF was normalized to baseline F (ΔF/F, applies to all panels in Figs. 6–7). **: $p < 0.01$, t test (compared to $Train_{10s}$ data in Ctrl).

(H) Applying MES solution (pH:5.5, bars) quenched F_{SypH} (mean + s.e.m.) to a similar level (dotted line) before and after $Train_{10s}$ in $Actb^{-/-}$ boutons (n = 6 experiments). ΔS represents pre-existing SypH molecules at the plasma membrane that can be quenched.

(I) F_{SypH} traces, $Rate_{decay}$ and ΔF (mean + s.e.m.) induced by $Train_{10s}$ in Ctrl (n = 4, black) or $Actb^{-/-}$ boutons (n = 5 experiments, red) at 34–37°C. Mean F_{SypH} traces were also scaled and superimposed (right). *: $p < 0.05$; **: $p < 0.01$, t test.

(J) F_{SypH} traces, $Rate_{decay}$ and ΔF (mean + s.e.m.) induced by a 10 s train at 80 Hz at 22–24°C in Ctrl (n = 4, black) or $Actb^{-/-}$ boutons (n = 5 experiments, red). Mean F_{SypH} traces were also scaled and superimposed (right). **: $p < 0.01$, t test.

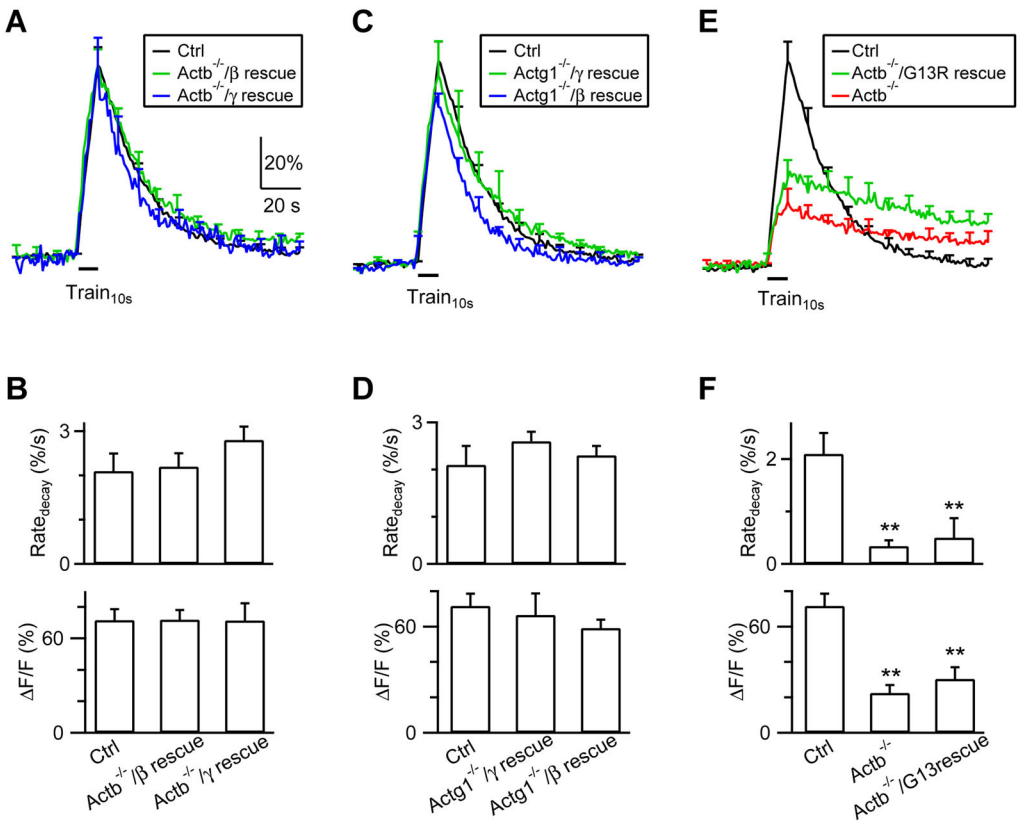

Figure 7. Actin polymerization is needed for endocytosis

(A–B) F_{SypH} traces (A), $Rate_{decay}$ and ΔF (B) induced by $Train_{10s}$ (bar) in Ctrl hippocampal boutons (n = 8 experiments), in $Actb^{-/-}$ boutons transfected with β-actin ($Actb^{-/-}$/β rescue; transfection of β-actin with SypH and a Cre-mCherry plasmid in $Actb^{LoxP/LoxP}$ boutons; n = 6), and in $Actb^{-/-}$ boutons transfected with γ-actin ($Actb^{-/-}$/γ rescue, n = 6). Data are expressed as mean + s.e.m.

(C–D) Similar to A–B, but for $Actg1^{-/-}$ boutons transfected with γ-actin ($Actg1^{-/-}$/γ rescue, n = 8) or β-actin ($Actg1^{-/-}$/β rescue, n = 8).

(E–F) Similar to panel A–B, but for Ctrl boutons (n = 8), $Actb^{-/-}$ boutons (n = 11), and $Actb^{-/-}$ boutons transfected with β-actin(G13R) [$Actb^{-/-}$/G13R rescue: transfection of β-actin(G13R) with SypH and a Cre-mCherry plasmid in $Actb^{LoxP/LoxP}$ hippocampal boutons; n = 8]. **: $p < 0.01$, t test.

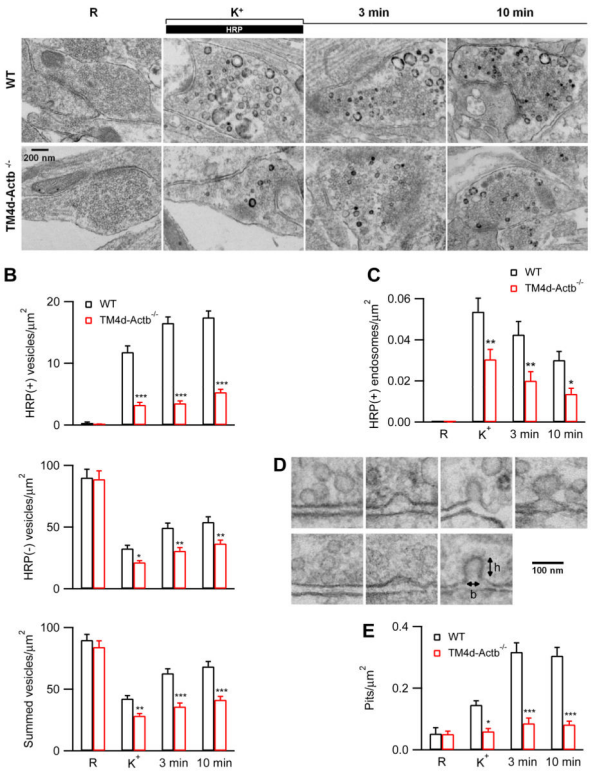

Figure 8. Ultrastructural changes in TM4d-Actb$^{-/-}$ hippocampal boutons

(A) EM images of wild-type and TM4d-Actb$^{-/-}$ hippocampal boutons fixed at rest (R) and at 0, 3 and 10 min after the end of 1.5 min 90 mM KCl application. For R, HRP was included for 1.5 min; for KCl application, HRP was included only during KCl application (see labels).

(B–C) The number of HRP(+) vesicles, HRP(−) vesicles, and their sum (B), and the bulk endosome area (C) per µm^2 of synaptic cross section are plotted versus the time before (R) and at 0 (K$^+$), 3, and 10 min after the end of KCl application in control and TM4d-Actb$^{-/-}$ hippocampal cultures (mean + s.e.m., each group was from 40–100 synaptic profiles). ***, $p < 0.001$; **, $p < 0.01$; *, $p < 0.05$ (ANOVA, also applies to E).

(D) EM images of membrane pits with various shapes obtained during or after KCl application from either control or TM4d-Actb$^{-/-}$ culture. h and b refer to pit height and base length.

(E) The number of pits before (R) and after KCl application in control and TM4d-Actb$^{-/-}$ synapses (mean + s.e.m.).